Journal of Volcanology and Geothermal Research 441 (2023) 107874

Contents lists available at ScienceDirect

Journal of Volcanology and Geothermal Research

journal homepage: www.journals.elsevier.com/journal-of-volcanology-and-geothermal-research

Evaluating bubble chain phenomena as a mechanism for open system degassing in basaltic systems

M. Lo [a,*], A. Loisel [b], M. Burton [a], E.W. Llewellin [b]

[a] Department of Earth and Environmental Sciences, University of Manchester, Oxford Road, Manchester M13 9PL, UK
[b] Department of Earth Sciences, Durham University, South Road, Durham DH1 3LE, UK

ARTICLE INFO

Keywords:
Viscoelastic
Hydroxyethyl cellulose
Cellosize
Bubble chains
Analogue experiments

ABSTRACT

Passive degassing – i.e., the open-system degassing of a magmatic gas phase that is decoupled from the melt phase – is common at many basaltic volcanic systems and consistently makes a greater contribution to total volcanic gas emissions than eruptive degassing. However, the mechanism for passive degassing is not fully understood. We investigate the feasibility of permeable gas flow through connected bubbles or pathways using experiments with aqueous solutions of hydroxyethyl cellulose (HEC), a non-Newtonian analogue material for magma. Stable chains of connected bubbles have previously been reported in similar non-Newtonian polymer solutions. We observe a range of bubble chain phenomena and identified five regimes, numbering in order of increasing gas flow rate: 1) small individual bubbles; 2) chains of rounded bubbles; 3) chains of elongate bubbles; 4) pipe-like 'winding flue'; 5) large individual bubbles. The bubble chain phenomena (regimes 2–4) are observed over a restricted interval of gas flow rates. We determine the rheology of the solutions and conclude that the HEC solutions that produced bubble chain phenomena in our experiments are well scaled to shear-thinning and viscoelastic magmas, hence bubble chain phenomena could form in magmas. Our analysis also suggests that the viscoelastic rheology of HEC plays a fundamental role in the observed bubble chain phenomena.

1. Introduction

Passive degassing consistently makes a greater contribution to overall volcanic emissions than eruptive degassing, contributing an average of 23 Tg SO_2 annually between 2005 and 2017, an order of magnitude greater than eruptive SO_2 (Carn et al., 2017). Passive magma degassing is a common feature of low viscosity basaltic magmatic systems, including Etna, Stromboli (Italy), Villarica (Chile), and Masaya (Nicaragua). In arc systems, the initial volatile content of basaltic magma may exceed 4 wt% due to the abundance of H_2O and CO_2 (Burton et al., 2007a; Blundy et al., 2010). If this magma were to ascend and degas within a closed system, in which all the exsolved gas stayed physically coupled with its parental magma, then the vesicularity of the final magma would exceed 99 vol%, and the total volume of gas at atmospheric pressure produced by 1 m^3 of magma may approach 1000 m^3 (Burton et al., 2007a). Instead, typical erupted lavas have vesicularities of ~50 vol% (Houghton and Wilson, 1989; Song et al., 2001), indicating that basaltic magma degasses dominantly as an open system, in which gas decouples from its parent melt and escapes at the surface quiescently. The precise nature of this decoupled passive gas flow is an important open research question because even a small degree of coupling between this voluminous gas flow and the melt could lead to explosive activity (Wilson and Head, 1981; Parfitt, 2004; Houghton and Gonnermann, 2008). Insights into the processes controlling degassing would also help in the interpretation of phenomena such as volcanic tremor, which might be produced during passive degassing (Salerno et al., 2018). Understanding the complete gas budget (passive and eruptive) at different volcanic systems is an important goal for effective volcanic gas monitoring (Francis et al., 1998; Galle et al., 2003), understanding explosive processes (Mori and Burton, 2009), eruption forecasting (Aiuppa et al., 2007), and volcanic gas hazard and risk assessments (Hansell and Oppenheimer, 2004; Van Manen, 2014).

Possible mechanisms for open-system degassing include ascent and bursting of gas bubbles, slug flow, and permeable gas flow through connected bubbles (Blackburn et al., 1976; Burton et al., 2007b; Burgisser and Degruyter, 2015; Mintz et al., 2021). In this study, we explore the feasibility of bubble chain phenomena as a mechanism for open-system degassing. Bubble chains are continuous strings of bubbles that

* Corresponding author.
E-mail addresses: marissa.lo@geolsoc.org.uk (M. Lo), ariane.loisel@durham.ac.uk (A. Loisel), mike.burton@manchester.ac.uk (M. Burton), ed.llewellin@durham.ac.uk (E.W. Llewellin).

https://doi.org/10.1016/j.jvolgeores.2023.107874
Received 29 April 2022; Received in revised form 20 July 2023; Accepted 21 July 2023
Available online 23 July 2023

do not detach from each other, but are connected by thin 'necks' at the top and bottom of each bubble. The phenomenon was first documented by Kliakhandler (2002), who observed bubble chains in experiments in which gas was continuously injected into a column of a concentrated solution of the polymer hydroxypropyl methyl-cellulose, which has a viscoelastic rheology. Kliakhandler (2002) suggested that the non-Newtonian, viscoelastic rheology of the solution was key in producing the bubble chain phenomena: in a viscoelastic fluid, such as a polymer solution, contraction at the rear of an ascending bubble is impeded by the elastic nature of the fluid, allowing a neck to form between bubbles; this does not happen in a Newtonian fluid. Divoux et al. (2009) conducted similar experiments using a viscoelastic hair gel and observed an additional regime of gas behaviour: a winding tube or flue of gas, connecting the point of gas injection to the surface of the hair gel. They also observed that the ascending gas would fluctuate between the bubble chain regime and winding flue regime spontaneously, without any change in gas flow rate. It was concluded that the non-Newtonian nature of the fluid was the key factor in producing the winding flue regime and inducing the fluctuations between regimes. This hypothesis was developed further in Divoux et al. (2011), where a critical flow rate for the transition between the two gas flow regimes to occur was identified, for certain concentrations of hair gel solution. Based on the viscoelastic properties of magma, Divoux et al. (2011) suggested that the observed gas flow regimes may play a role in passive degassing at basaltic volcanoes.

We explore the feasibility of the hypothesis that bubble chains and winding flues may play a role in magmatic outgassing by: (1) identifying the conditions at which bubble chains and winding flues occur within hydroxyethyl cellulose (HEC) solution, a relatively well-understood viscoelastic analogue material for magma (Naik et al., 1976; Jones et al., 2020); (2) characterising the rheology of the HEC solutions in which bubble chains and winding flues form; and (3) relating the rheology of the HEC solutions to basaltic magmas and volcanic systems. To achieve these aims, we conducted experiments in which gas was injected continuously into the bottom of a pipe filled with HEC solution. HEC solution concentration, gas injection rate, pipe size, and injection nozzle size were varied. Observations were made for both increasing and decreasing gas injection rates, in order to determine whether the system showed any hysteresis. Once we identified HEC solution concentrations that produced bubble chains and winding flues, the final aim was to relate their rheology to that of magma (Jones et al., 2020).

2. Material and methods

2.1. Preparation and properties of hydroxyethyl cellulose solutions

HEC is a water-soluble polymer, comprising large molecular chains (Del Giudice et al., 2017), which is used commercially as a thickening agent and rheological modifier for a wide range of products. The rheology of HEC solution depends on the concentration of the solution and the temperature (Naik et al., 1976; Del Giudice et al., 2017; Jones et al., 2020). In-depth studies of the rheological properties of HEC solutions are mostly driven by the need to understand how HEC affects the stability and properties of the products it is used in (Dinic and Sharma, 2020). In this study, we used a commercially available brand of HEC: Cellosize QP 52000H, manufactured by DOW.[1] The HEC in this product has a molecular weight of 150,000 g mol^{-1}. Aqueous solutions of HEC with differing concentrations were made in small batches, following the procedure in Jones et al. (2020), by adding the required amount of powdered Cellosize to hot water, ranging from 54 to 57 °C in temperature, to facilitate the dissolution of the HEC powder. Five different concentrations, X, of HEC solution were made: $X = 0.75$, 1.0, 1.2, 1.5, and 1.7 wt% (where, for the avoidance of ambiguity, a solution of 1 g of HEC in 99 g of water has a concentration of 1 wt%). The choice of concentration was guided by the concentrations of hydroxypropyl methyl-cellulose solution used by Kliakhandler (2002).

Aqueous solutions of HEC have a shear-thinning rheology (Maestro et al., 2002; Jones et al., 2020), meaning that the apparent viscosity η [Pa] decreases with increasing strain rate $\dot{\gamma}$ [s^{-1}]. At low strain rate, the chains tumble at random, resisting flow and raising the viscosity of the solution; with increasing strain rate, the molecules become increasingly aligned with flow, decreasing the viscosity of the solution towards that of the solvent. HEC solutions do not show a yield stress (Naik et al., 1976). Jones et al. (2020) characterize the rheology of solutions of Cellosize QP 52000H (the same product that we use in the current study) and find that it is well described by a Cross model:

$$\eta = \eta_\infty + \frac{\eta_0 - \eta_\infty}{1 + (c\dot{\gamma})^p} \tag{1}$$

where η_0 is the asymptotic zero-strain-rate viscosity, η_∞ is the solvent viscosity (in this case water), c is the Cross constant, and p is the Cross exponent. Their study spans the range of concentrations that we use and provides empirical correlations for the coefficients of the Cross model (c and p), which we use to plot apparent viscosity of our solutions as a function of strain rate, in Fig. 1a.

Dinic and Sharma (2020) investigate the rheology of solutions of HEC with a range of molecular weights and find that the dependence of the specific viscosity $\eta_{sp} = (\eta_0 - \eta_\infty)/\eta_\infty$ of a solution on its concentration has three different regimes: a dilute regime in which $\eta_{sp} \propto X$; a semi-dilute regime in which $\eta_{sp} \propto X^2$; and a concentrated or 'entangled' regime in which $\eta_{sp} \propto X^{4.3}$. Using the results in Table 1 of Jones et al. (2020) we find that $\eta_{sp} \propto X^{4.8}$ for solutions of Cellosize QP 52000H over the range $0.75 \leq X \leq 1.75$ at 20 °C, which is in good agreement with the value proposed by Dinic and Sharma (2020) for the concentrated regime (Fig. 1b).

HEC solutions also show viscoelastic behaviour, where the strain associated with deformation may be both elastic and viscous: i.e., recoverable and non-recoverable. We characterize the viscoelastic rheology (Fig. 2) of three HEC solutions: $X = 1.5$, and 1.7 wt%, which both show bubble chain phenomena (see Section 3 later); and $X = 1.2$ wt %, which is the highest concentration that does not. The rheology of the solutions is measured with a Thermo Scientific HAAKE rheometer (Viscotester iQ Air) at 20 °C, which is the approximate ambient laboratory temperature during the bubble flow experiments, using a fully immersed concentric cylinder geometry (CCB25 DIN sensor geometry). Frequency sweeps (Figs. 2b-d) are conducted at stress amplitude $\tau_0 = 5$ Pa, which is within the linear viscoelastic region (LVE) for all solutions (Fig. 2a). Results for frequencies above around 10 Hz (i.e. for $\omega \gtrsim 20\pi$ rad/s) are increasingly influenced by the inertia of the sensor geometry and are not plotted. Fig. 2c plots both complex viscosity against angular frequency under oscillatory rheometry, and apparent viscosity against strain rate under rotational rheometry, using the same sensor system, confirming that the HEC solutions we use follow the Cox-Merx rule, on which we rely later, in Section 4, when we explore the analogy between our experiments and behaviour in bubbly magmas (Cox and Merz, 1958; Mader et al., 2013; Jones et al., 2020).

We are primarily interested in the rheology of the HEC solutions over the interval of stresses, strain rates, and frequencies of deformation that are imparted on them by the bubble chain phenomena. In the Appendix, we estimate the range of stresses arising from bubble buoyancy, and the consequent range of strain rates in the solutions. These ranges are plotted on Fig. 2c and are considered in the discussion in Section 4.

2.2. Bubbling experiments

The experimental set up consisted of a vertical, cylindrical Perspex pipe, mostly filled with HEC solution (Fig. 3). Compressed air was injected continuously into the solution at the base of the pipe, first

[1] https://www.dow.com/en-us.html

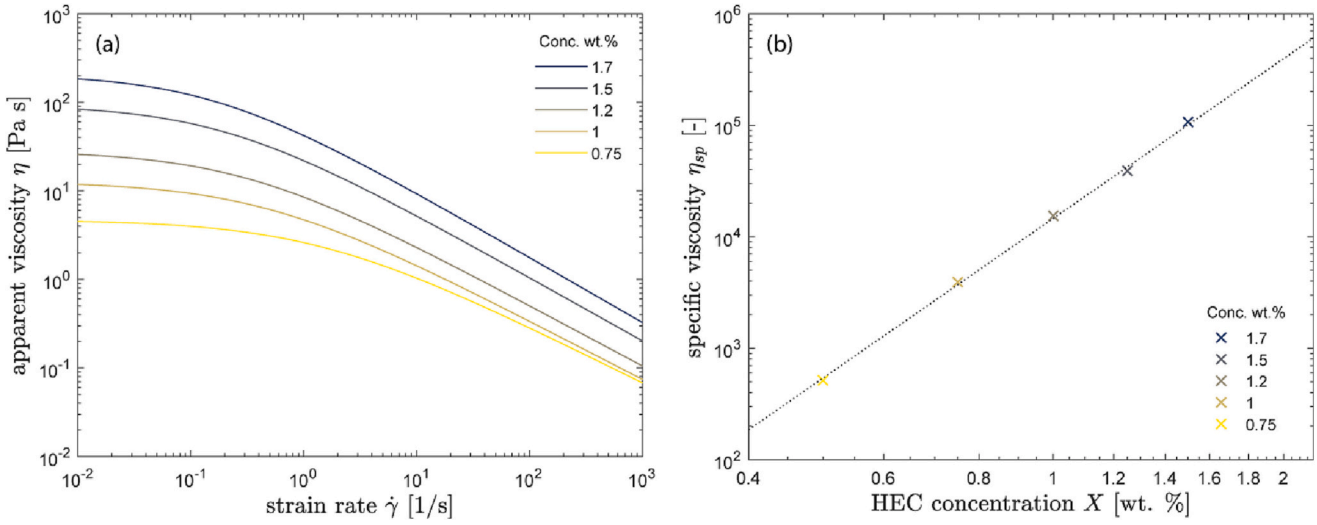

Fig. 1. (a) Apparent viscosity η as a function of strain rate $\dot{\gamma}$ for different concentrations X of HEC solution. Curves are calculated following Jones et al. (2020). (b) Specific viscosity η_{sp} as a function of concentration X for HEC solutions at 20 °C. Values are calculated from experimental data taken from Table 1 of Jones et al. (2020). Best fit power law (dotted line) is $\eta_{sp} = 1.46 \times 10^4 X^{4.76}$.

Table 1
Experiment variables. HEC concentration, pipe size, and nozzle size were varied discretely at the values stated. Gas flow rate was varied continuously within the range, in increments of 0.02 L min^{-1}.

Variable	Range of values (and increments)	Units
HEC concentration	0.75, 1.0, 1.2, 1.5, and 1.7	weight %
Gas flow rate	0.0–0.5 (increments of 0.02)	L min^{-1}
Pipe inner diameter	3.0, 6.5, and 9.5	cm
Nozzle inner diameter	3, 4, and 7	/32nds of an inch
	(=2.38, 3.175, and 5.56)	(mm)

through an Omega FL-2010 flowmeter, which limited gas flow rates to 0.1 to 0.5 L min^{-1}, then through an on/off tap, and into a narrow copper injection nozzle that protruded vertically into the solution. HEC solution is colourless and near-transparent so movement of gas through the solution can be clearly observed. Similar shear-thinning solutions have been used in previous studies of bubble dynamics, such as hydroxypropyl methyl-cellulose (Kliakhandler, 2002), commercial hairdressing gel (Divoux et al., 2009), and sodium salicylate and hexadecyltrimethylammonium bromide mixture (Vidal et al., 2011).

Four variables were changed throughout the experiments: (1) HEC solution concentration, (2) gas flow rate, (3) pipe diameter, and (4) gas injection nozzle diameter. The range of values used for each of these variables is summarised in Table 1. We varied flow rate to reflect changes in natural volcanic systems and to determine how sensitive the flow phenomena are to flow rate variation. We investigated the effect of HEC concentration to reflect changes in viscosity, hence rheology. Pipe diameter was varied to see whether the walls of the pipe would influence flow phenomena, analogous to conduit walls in natural magmatic systems. Lastly, while gas injection nozzle diameter does not have an equivalent in natural volcanic systems, we varied this over a factor of roughly 2 to determine whether this had an effect on the flow phenomena.

Once a prepared HEC solution had cooled, it was poured into the Perspex pipe. During pouring, bubbles were often incorporated into the solution, so the solution was left to settle in the pipe for at least an hour before starting an experiment; this allowed time for bubbles to ascend or dissolve, though some small bubbles remained in the upper part of the pipe, and for the solution to reach ambient laboratory temperature.

Each experiment consisted of incrementally increasing the flow rate of the gas injected into the HEC solution, whilst monitoring associated bubble behaviour. Starting from zero flow rate, gas flow rate was increased by approximately 0.02 L min^{-1}, roughly every 10–20 s, to a maximum gas flow rate of 0.5 L min^{-1}. Gas flow rate was then decreased, in the same fashion, from 0.5 L min^{-1} back to zero flow rate. Written observations of bubble size, shape, stability, and relationship to other bubbles were made at each increment of gas flow rate. Photographs were captured at regular intervals, as well as video recordings of each experiment run. Observations were generally made within the bottom half of the Perspex pipe, to avoid any confounding effect of bubbles that remained in the solution following pipe filling, which were more common at the top of the pipe. Experiments were conducted at ambient laboratory temperature, which was recorded, and varied in the range 22.2–24.1 °C.

3. Results

3.1. Observations of gas flow regimes

Six gas flow regimes were identified (Fig. 4) based on qualitative phenomenology. The same regimes were observed sequentially during all experiments. Results were recorded by noting the gas flow rate, observations of the gas flow regime, and interpreted gas flow regime. Numbers 1 to 5 were used, with the occasional .5 noted when behaviour was judged to be intermediate between two regimes. For example, a flow regime was classified as a 2.5 when bubbles in the chain were roughly 50% spherical/bead-like and 50% elongate/rice grain-like.

It should be noted that, due to refraction, the observed size of features in the HEC differs from the actual size of the feature. This discrepancy was greatest at the edge of each pipe, with a 5% difference between the observed and actual width in the 3 cm diameter pipe, 10% difference in the 6.5 cm pipe, and a 15% difference in the 9.5 cm pipe. The observed widths of different features are reported in this section.

3.1.1. Flow regime 0

Flow regime 0 was observed at the start of each experiment and describes the absence of gas emerging from the gas injection nozzle. On commencing an experimental run, a certain build-up of gas pressure was needed before gas would flow through the nozzle and form bubbles. This likely arises from surface tension at the nozzle because HEC does not have a yield stress (Naik et al., 1976). This behaviour led to an observed minimum gas flow rate of roughly 0.025 L min^{-1}, above which gas flow was not impeded.

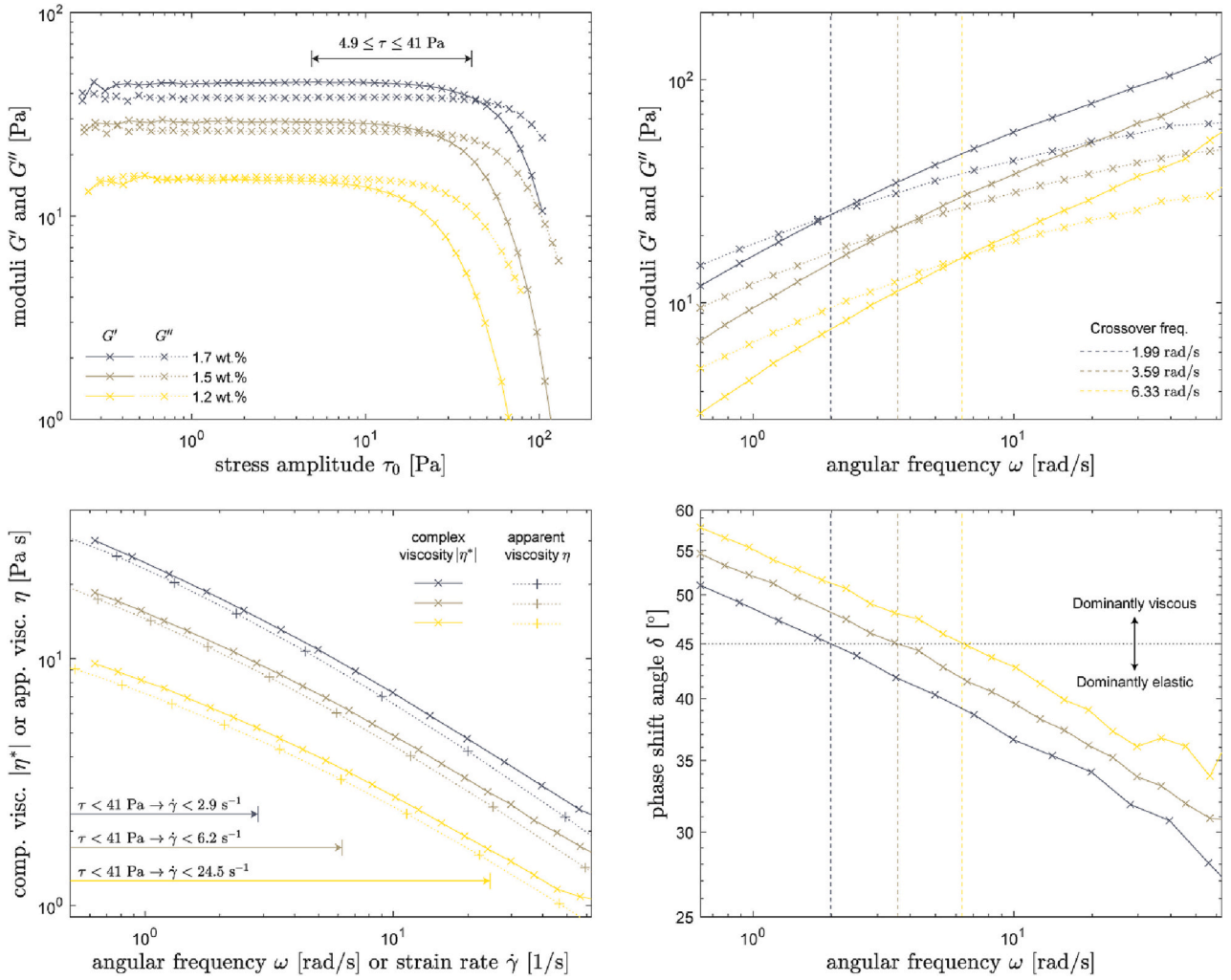

Fig. 2. Oscillatory rheology of three HEC solutions used in this study, conducted at 20 °C. (a) Stress amplitude sweep, conducted at a frequency of 1 Hz, showing that the linear viscoelastic region is bounded by $\tau_0 \lesssim 30$ Pa. Line indicates the range of maximum buoyancy stresses exerted on the fluid by the bubbles in our experiments (see Appendix). (b) Frequency sweep at $\tau_0 = 5$ Pa. Vertical lines indicate the angular frequencies at which G' and G'' cross for each solution. (c) Complex viscosity modulus as a function of angular frequency under oscillatory rheometry, and apparent viscosity as a function of strain rate under rotational rheometry. Arrows indicate the estimated upper limit of strain rate associated with the buoyancy stress exerted by the largest bubbles in our experiments (see Appendix). (d) Phase shift angle as a function of angular frequency. Vertical lines are the same as in (b) and represent $\delta = 45°$, which divides dominantly viscous and dominantly elastic behaviour. The colour scale shown in the legend of (a) indicates solution concentration in all plots. Note that lines joining data points are presented to help guide the eye and are not model fits.

3.1.2. Flow regime 1

Once gas began flowing through the gas injection nozzle, gas ascended as individual bubbles, with no bubble chain forming (Fig. 4, panel 1). Individual bubbles were 2.5–3.0 cm in height and 1.5–2.0 cm in width at the widest point, with an average height:width ratio of roughly 1:0.65. The individual bubbles were tapered at the trailing edge, giving the bubbles a hot air balloon-like shape. Approximately a third to a half of the bubbles coalesced with a bubble above it, forming a larger bubble roughly 3.0–3.5 cm in height and 2.0–2.5 cm in width, again giving an average height:width ratio of roughly 1:0.65. The coalesced bubbles ascended more quickly within the HEC, due to their greater volume, hence buoyancy, which led to further bubble coalescence. At the base of the pipe, before any bubble coalescence, individual bubbles were spaced roughly 1 cm apart. Individual bubbles were produced at the gas injection nozzle at an approximate rate of 1 s^{-1}.

3.1.3. Flow regime 2

As gas flow rate was increased, the second gas flow regime was observed (Fig. 4, panel 2): an individual bubble of the sort described in regime 1 would produce a chain of bubbles from its narrow tail. The chain consisted of a repeating sequence of rounded bubbles, ~8 mm in height and ~6 mm in width, with an average height:width ratio of roughly 1:0.75. The connecting neck between neighbouring bubbles was much thinner, with a width of 1–2 mm. The width of bubbles along the chain appeared to vary temporally, giving the impression that gas was not ascending through the chain in a completely uniform way. The chain extended the full height of the HEC solution, from the gas injection nozzle to the surface of the HEC. Individual bubbles would ascend slowly (a couple of mm per second, depending on the gas flow rate) up the pipe, connected to other bubbles at the head and base, in a conveyor belt-like fashion from the gas injection nozzle. Bubbles in the chain would ascend more quickly when gas flow rate was increased, since an increase in gas flow rate resulted in a greater rate of bubble production at the nozzle.

As long as gas flow rate was relatively constant (not altered suddenly by 0.1 L min^{-1} or more), the chain of bubbles was very stable. If gas flow rate was suddenly altered, the chain would separate, with the necks between the bubbles closing up, leaving individual stationary bubbles

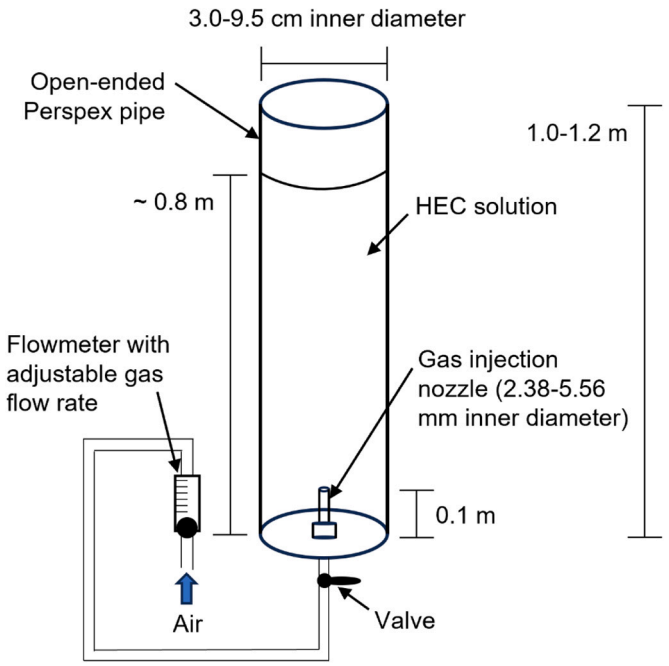

Fig. 3. Experiment set-up for observing gas flow within hydroxyethyl cellulose solution (HEC). Experiment set-up consisted of an upright Perspex pipe, partly filled with HEC solution, with air injected into the base of the pipe using a gas injection nozzle. Gas flow rate was controlled by a flowmeter.

suspended within the HEC.

3.1.4. Flow regime 3

As gas flow rate was increased once more, the third gas flow regime was observed (Fig. 4, panel 3): the roughly-spherical bubbles observed in regime 2 gradually became narrower and longer. The chain was made up of a repeating pattern of elongate, rice grain-shaped bubbles, ~8–10 mm in height and ~ 4 mm in width, with an average height:width ratio of roughly 1:0.5. The connecting neck between adjacent bubbles appeared to be the same as flow regime 2, with a width of 1–2 mm. Again, the width of bubbles along the chain appeared to vary temporally, giving the impression that gas was not ascending through the chain in a completely uniform way. The chain continued to extend from the gas injection nozzle to the surface of the HEC. Individual bubbles would ascend and eventually reach the surface of the HEC, in the same manner as described for flow regime 2. Bubbles ascended slowly, ascending roughly a couple of mm per second, depending on the gas flow rate.

Similar to flow regime 2, as long as gas flow rate was kept relatively constant (not altered suddenly by 0.1 L min^{-1} or more), the chain of bubbles was very stable. If gas flow rate was suddenly altered, the chain would separate, with the necks between the bubbles closing up, leaving individual bubbles stationary in the HEC.

3.1.5. Flow regime 4

Continued increase in gas flow rate brought about a fourth gas flow regime (Fig. 4, panel 4). This flow regime was characterised by a change to a continuous pipe-like 'winding flue' of gas. The necks between individual bubbles disappeared, becoming indistinguishable from the walls of the individual bubbles. The thickness of the flue varied vertically, between 3 and 5 mm in width. When gas flow rate was constant, the flue was stable. However, if there were any stationary bubbles within the HEC, the flue was likely to break down when it met the bubble, resulting in the formation of individual bubbles with the same characteristics as in flow regime 1. The flue was also static, with the gas consistently using the same path through the HEC. Flow regime 4 did not have the same undulating appearance of flow regimes 2 and 3, instead, the gas seemed to ascend more uniformly through the flue. A notable characteristic of this gas flow regime was a draining or whistling sound, which fluctuated slightly in volume, originating from the gas moving through and escaping from the surface of the HEC.

3.1.6. Flow regime 5

Finally, the fifth gas flow regime initiated when the head of the continuous flue began to break down into individual bubbles (Fig. 4, panel 5). This would begin at the top of the flue then, as gas flow rate was increased, the point at which the flue would break into individual bubbles propagated down the flue, until the entire flue had broken down and individual bubbles formed at the gas injection nozzle. The bubbling behaviour was the same as in flow regime 1, however, the individual bubbles were slightly larger and more elongated than those observed in flow regime 1. Individual bubbles were 3.5–4.5 cm in height and 2.0–2.5 cm in width at the widest point, with an average height:width ratio of roughly 1:0.6. The individual bubbles were tapered at the end, giving the bubbles a hot air balloon-like shape. Approximately half of the bubbles coalesced with a bubble above it, forming a larger bubble roughly 5.0–5.5 cm in height and 2.5–3.0 cm in width, again giving an average height:width ratio of roughly 1:0.55. The coalesced bubbles ascended more quickly within the HEC, due to their greater volume, hence buoyancy, which led to further bubble coalescence. At the base of the pipe, before any bubble coalescence, individual bubbles were spaced roughly 0.5 cm apart – more closely than the individual bubbles observed in flow regime 1. Individual bubbles were produced at the gas injection nozzle at an approximate rate of 2.5 s^{-1}.

3.2. Occurrence of gas flow regimes

The complete range of gas flow regimes described above was only observed in the 1.5 and 1.7 wt% HEC solutions. For the 0.75, 1.0, and 1.2 wt% HEC solutions, only gas flow regime 1 was observed (Table 2).

For a 1.7 wt% HEC solution, bubble chains (flow regime 2) would start forming between 0.10 and 0.16 L min^{-1}; transition to flow regime 3 would occur between 0.18 and 0.22 L min^{-1}; transition to the winding flue of flow regime 4 occurred between 0.24 and 0.34 L min^{-1}; finally, the breakdown of flow regime 4 into flow regime 5 occurred between 0.42 and 0.50 L min^{-1} (Fig. 5). Of the four variables tested, only gas flow rate and HEC concentration affected the occurrence of different gas flow regimes (Fig. 5).

Pipe size did not affect the occurrence of different bubble flow regimes, but when using the smallest pipe (3.5 cm diameter), flow regimes 2–4 appeared to be less stable. When using the smallest pipe, with an increasing gas flow rate, the chains of bubbles and the flue were more prone to breaking into individual bubbles partway up the structure. As long as gas flow rate was kept relatively constant (no sudden changes of 0.1 L min^{-1} or greater), bubble chains were stable over the measurement period in 90% of the cases for the larger pipes, but were only stable over the measurement period in 50% of the cases for the smallest pipe. Once it had destabilised, the chain or flue would then re-establish within a few seconds. The diameter of the injection nozzle did not have a noticeable impact on bubble flow regime. Individual bubbles and chain-like features appeared to form in the same way for all injection nozzle sizes used.

In each experiment run, gas flow rate was increased and decreased incrementally to determine whether the occurrence of a bubble flow regime would differ depending on the preceding gas flow rate. In both of the solutions (1.5 and 1.7 wt% HEC solution) where all five bubble flow regimes were observed, systematic hysteresis was not observed (Fig. 6). In Fig. 6, we present experiment runs 20190822A and 20190822C, which show typical behaviour, and had the following experiment conditions: 1.5 wt% HEC, 6.5 cm diameter pipe, 2.38 mm inner diameter gas injection nozzle. We also present results from 4 other experiment runs to show the effect of varying HEC concentration, pipe diameter, and

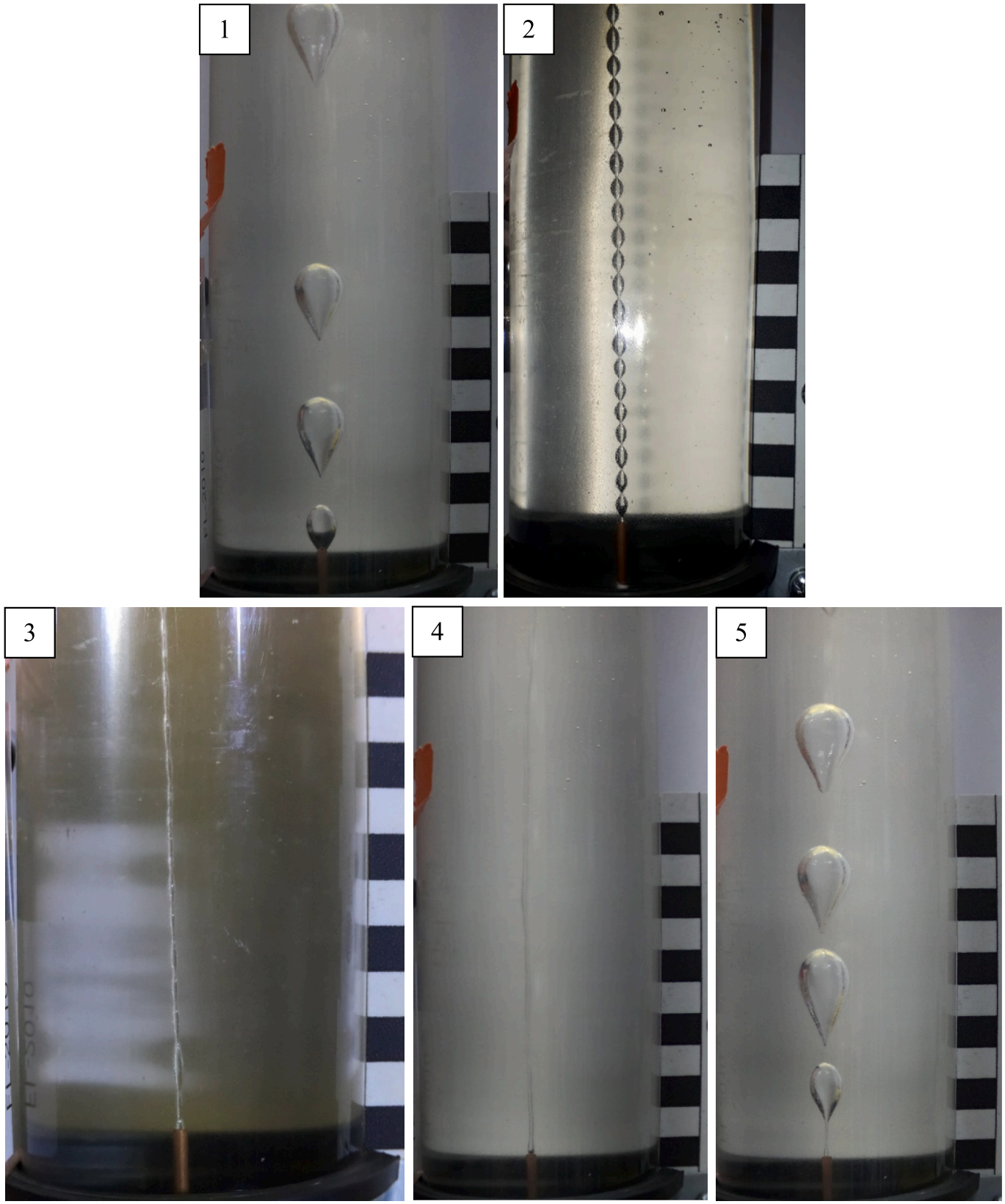

Fig. 4. Photographs of each bubble flow regime described in Section 3.1. All images are from an experiment with 1.7 wt% HEC solution, a 6.5 cm diameter pipe, and a gas injection nozzle with an inner diameter of 2.38 mm. Number in top left corner of each panel indicates flow regime number. Black and white ruler markings mark 1 cm. Note: scale is not consistent across figure, in order to highlight the key characteristics of each flow regime clearly.

Table 2
Summary of all experiment parameters and the range of observed gas flow regimes. For each experiment, HEC concentration, pipe inner diameter, and nozzle inner diameter are stated, as well as the resulting gas flow regimes observed. Experiments marked with an asterisk did not produce bubble chain behaviour. Note: experiment 20190821B is omitted due to a gas leak partway through the experiment.

Experiment Name	HEC concentration/ wt%	Inner diameter of pipe/cm	Inner diameter of gas injection nozzle/mm	Gas flow regimes observed
20190819A	1.7	6.5	2.38	1–5
20190819B	1.7	6.5	2.38	1–5
20190819C	1.7	6.5	2.38	1–5
20190819D	1.7	6.5	2.38	1–5
20190820A	1.7	6.5	2.38	1–5
20190820B	1.7	3.0	2.38	1–5
20190820C	1.7	3.0	2.38	1–5
20190820D	1.7	3.0	2.38	1–5
20190820E*	0.75	6.5	2.38	1
20190821A	1.7	3.0	2.38	1–5
20190821C*	1.0	6.5	2.38	1
20190821D*	1.2	6.5	2.38	1
20190821E	1.7	9.5	2.38	1–5
20190822A	1.5	6.5	2.38	1–5
20190822B	1.5	6.5	2.38	1–5
20190822C	1.5	6.5	2.38	1–5
20190822D	1.7	9.5	2.38	1–5
20190822E	1.7	9.5	2.38	1–5
20190822F	1.7	9.5	2.38	1–5
20190822G	1.7	9.5	2.38	1–5
20190822H	1.7	6.5	3.175	1–5
20190823A	1.7	6.5	3.175	1–5
20190823B	1.7	6.5	5.56	1–5
20190823C	1.7	6.5	5.56	1–5

gas injection nozzle size. During the increase and decrease of the gas injection rate, all gas flow regimes were observed; however, the gas injection rate transition point between the gas flow regimes varied. It is difficult to fully quantify how the preceding gas injection rate affected the gas flow regime and the point at which the next gas flow regime would occur, due to the fact that (1) the gas flow rate was being controlled manually and (2) some transitions were gradational rather than discrete. Overall, there did not seem to be a clear, systematic relationship between the preceding gas flow rate and the gas flow regime observed, and we conclude that minor stochastic variability may be responsible for regime transition variation, rather than any systematic factor.

4. Discussion

4.1. Bubble chain behaviour

We observed bubble chain behaviour in two of the solutions tested: the 1.5 wt% and 1.7 wt% HEC solutions. However, bubble chains did not form in the HEC solutions of lower concentrations (0.75, 1.0, and 1.2 wt %). When combined with the rheometry data, this suggests that the viscoelasticity of the material is an important factor in facilitating the formation of bubble chains, as suggested by Kliakhandler (2002) and Divoux et al. (2011). We infer that the bubbles in our experiments exerted stresses on the fluid, arising from their buoyancy, that fall almost exclusively within the linear viscoelastic region (see Fig. 2a and Appendix). Based on Fig. 5, our results suggest that an HEC concentration of 1.3 wt% may be the threshold for connected bubbles (gas flow regimes 2, 3, or 4) to form, however, further experiments would be needed to demonstrate this.

The diameter of the Perspex pipe did not make a difference to the type of bubble flow regimes observed, although it did affect the stability of the bubble chain or flue present: chains and flues were less stable in the smallest pipe. We speculate that stability may be influenced by the proximity of the pipe walls. It has previously been observed that the proximity of walls stabilizes the ascent of individual bubbles up pipes (Clift et al., 1978; James et al., 2011) which might favour regime 1 and regime 5, thereby destabilizing the bubble chain and winding flue regimes (2–4). The effect of pipe diameter on bubble stability was difficult to quantify using the method used here, where a number was assigned at each gas flow rate to describe the bubble flow regime. In order to quantitatively study the effect of pipe size, a method involving counting the number of times the bubble chain or flue broke down into individual bubbles in a given period of time could be adopted.

From quantitative and qualitative observations, the diameter of the injection nozzle did not seem to make a difference to bubble flow regime. It may be that a larger range of injection nozzle diameters needs to be tested in order to understand whether this has an effect on bubble flow regime. Although we identified the transition point between gas flow regimes in terms of gas flow rate, our observations were all made when incrementally increasing and decreasing gas flow rate. The effect of immediately injecting air at a certain gas flow rate, for example, at a rate of 0.14 L min^{-1}, the observed transition point between gas flow regime 1 and 2, was not observed but could provide further information on whether a degree of hysteresis exists in the system.

Comparisons between the work of Kliakhandler (2002) and Divoux et al. (2009, 2011) and our work can also be drawn. The bubble chains identified by Kliakhandler (2002) appear to correspond to our bubble flow regime 2. Meanwhile, the two gas flow regimes identified by Divoux et al. (2009) – the individual bubbles and the continuous flue – appear to correspond to our gas flow regimes 1 and 4 respectively. In this way, our work places both sets of observations within a more complete phenomenological framework.

4.2. Analogy with bubbly magma

Previous work has indicated that the bubble chains that are our main focus arise because of viscoelastic behaviour in the liquid (Kliakhandler, 2002; Divoux et al., 2009). Consequently, the success of the analogy between HEC and bubbly magma depends upon matching the balance of viscous and elastic behaviour of the two fluids. We therefore seek to quantify the properties of a bubbly magma that has the same viscoelastic behaviour as the HEC over the relevant conditions of shear.

Bubbly magma is shear thinning and viscoelastic (Llewellin et al., 2002; Rust et al., 2003; Mader et al., 2013). The Cox–Merz rule (Cox and Merz, 1958), which has previously been shown to apply to both bubble suspensions and HEC (Mader et al., 2013; Jones et al., 2020), postulates an empirical equivalence between shear thinning and viscoelastic behaviour for a fluid that shows both. It states that the dependence of the apparent viscosity on strain rate $\eta(\dot{\gamma})$ under shear thinning behaviour is empirically equivalent to the dependence of the magnitude of the complex viscosity on angular frequency of oscillation $|\eta^*|(\omega)$ under viscoelastic behaviour. Fig. 2 shows that the HEC solutions that supported bubble chain phenomena adhere closely to the Cox-Merz rule over the interval of stresses, and consequent strain rates, that we infer arise from the buoyancy of the bubbles. Furthermore, that interval also falls almost wholly within the regime in which viscous behaviour dominates over elastic (i.e., phase shift $\delta \gtrsim 45°$; Fig. 2d). This is important for the analogy with bubbly magma because bubbly liquids have been shown to have a dominantly viscous rheology (Llewellin et al., 2002).

Shear thinning behaviour in magma is captured by the capillary number $Ca = \lambda\dot{\gamma}$ and viscoelastic behaviour by the dynamic capillary number $Cd = \lambda\ddot{\gamma}/\dot{\gamma} = \lambda\omega$ (where $\lambda = \mu a/\Gamma$ is the bubble relaxation time, μ [Pa s] is the Newtonian melt viscosity, a [m] is the bubble radius, Γ [N/m] is the surface tension, and $\dot{\gamma}$ and $\ddot{\gamma}$ are respectively the strain rate and rate of change of strain rate). For bubbly magma, therefore, the Cox-Merz rule manifests as an equivalence between $\eta_r(Ca)$ and $\eta_r(Cd)$ where η_r is the apparent viscosity (shear thinning) or complex viscosity (viscoelastic) normalized by the melt viscosity. Jones et al. (2020) define

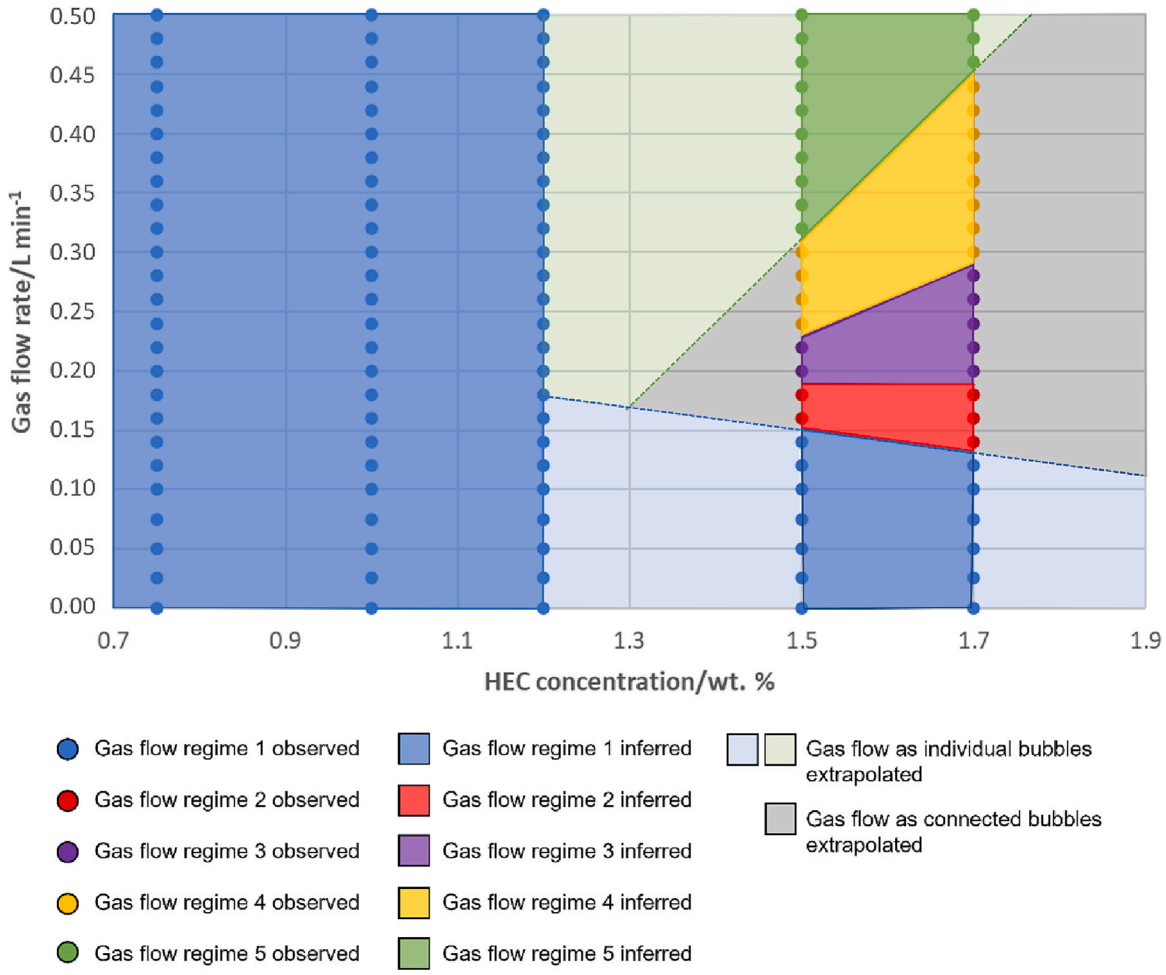

Fig. 5. Phase diagram showing gas flow regime based on gas flow rate and HEC concentration. Solid points show that the gas flow regime was observed at those conditions. Solid colours show the inferred gas flow regime. Pale colours show whether gas flow would occur as individual bubbles (gas flow regimes 1 and 5) or as connected bubbles (gas flow regimes 2, 3, and 4) extrapolated from the results.

a similar dimensionless quantity for HEC under shear thinning: $\eta_n(N_c)$, where η_n is the dimensionless relative viscosity, $N_c = c\dot{\gamma}$ is the dimensionless Cross number, and c is the Cross constant (see Jones et al., 2020 for details). By analogy, and via the Cox–Merz rule, we define a similar quantity for viscoelastic behaviour: $\eta_n(\lambda_m\omega)$ where λ_m is the Maxwell relaxation time, which is approximately equivalent to the Cross constant (Jones et al., 2020). We exploit the equivalence between $\eta_r(Ca)$ and $\eta_r(Cd)$, and between $\eta_n(N_c)$ and $\eta_n(\lambda_m\omega)$, that is implied by the Cox–Merz rule, in order to adopt the scaling approach developed by Jones et al. (2020) for HEC and bubbly magma.

We estimate the maximum frequency of oscillation for the HEC experiments (~10 Hz based on acoustic observations – the draining or whistling noise described in Section 3.1), convert this to angular frequency, and multiply by λ_m (Fig. 7) to determine the upper limit of the dimensionless frequency $\lambda_m\omega$. Via the Cox-Merz rule we take this as equivalent to the upper value of the product $N_c = c\dot{\gamma}$ under shear thinning. Following Jones et al. (2020) we then equate this upper value of N_c with the upper value of the capillary number Ca for an equivalent bubbly magma (accounting for a factor 6/5 since $N_c \equiv KCa$, where $K = 6/5$). We use the spreadsheet provided by Jones et al. (2020) to find the properties of a bubbly magma that has a $\eta_r(Ca)$ curve that is well matched to the $\eta_n(N_c)$ for the HEC over the appropriate range of Ca and N_c. A worked example is presented in the Supplementary Information.

A good approximate agreement between the shapes of the HEC and magma viscosity curves output by the model (Fig. 7 and Fig. S1 in the Supplementary Information) was found over the Ca range of interest. The results show that at $T = 20$ °C, the behaviour of the material over the range of concentrations tested (1.2 to 2.5 wt% HEC) is qualitatively similar to that of a magma with a relatively high gas volume fraction of $\varphi = 0.6$, with polydisperse bubble size distribution (polydisversity index = 1; Mader et al., 2013; Jones et al., 2020). It is thus suited for simulating shear-thinning and viscoelastic magmas.

This analysis suggests that the bubble flow experiments with HEC include fluid dynamic timescales over which shear thinning and viscoelastic behaviour are important, and we infer that shear-thinning and viscoelasticity play a fundamental role in the observed bubble chain phenomena. For magmatic systems this equates to processes that span low-to-high Ca and Cd (values)

4.3. Bubble chain phenomena in volcanic systems

Here we evaluate the applicability of our experiments, hence results, to real volcanic systems and identify complexities of natural systems that we have not been able to emulate. Divoux et al. (2011) suggested that gas flow phenomena, such as bubble chains, may explain passive degassing in basaltic volcanic systems. Our central finding is that bubble chain and winding flue phenomena can be produced, repeatably, in a material that has a viscoelastic rheology that is well scaled to bubbly magma. Divoux et al. (2011) further proposed that the non-Newtonian properties of magma would produce different modes of gas flow through the magma: as individual bubbles or as flue-like structures. The clear question that remained after the Divoux et al. (2011) study was

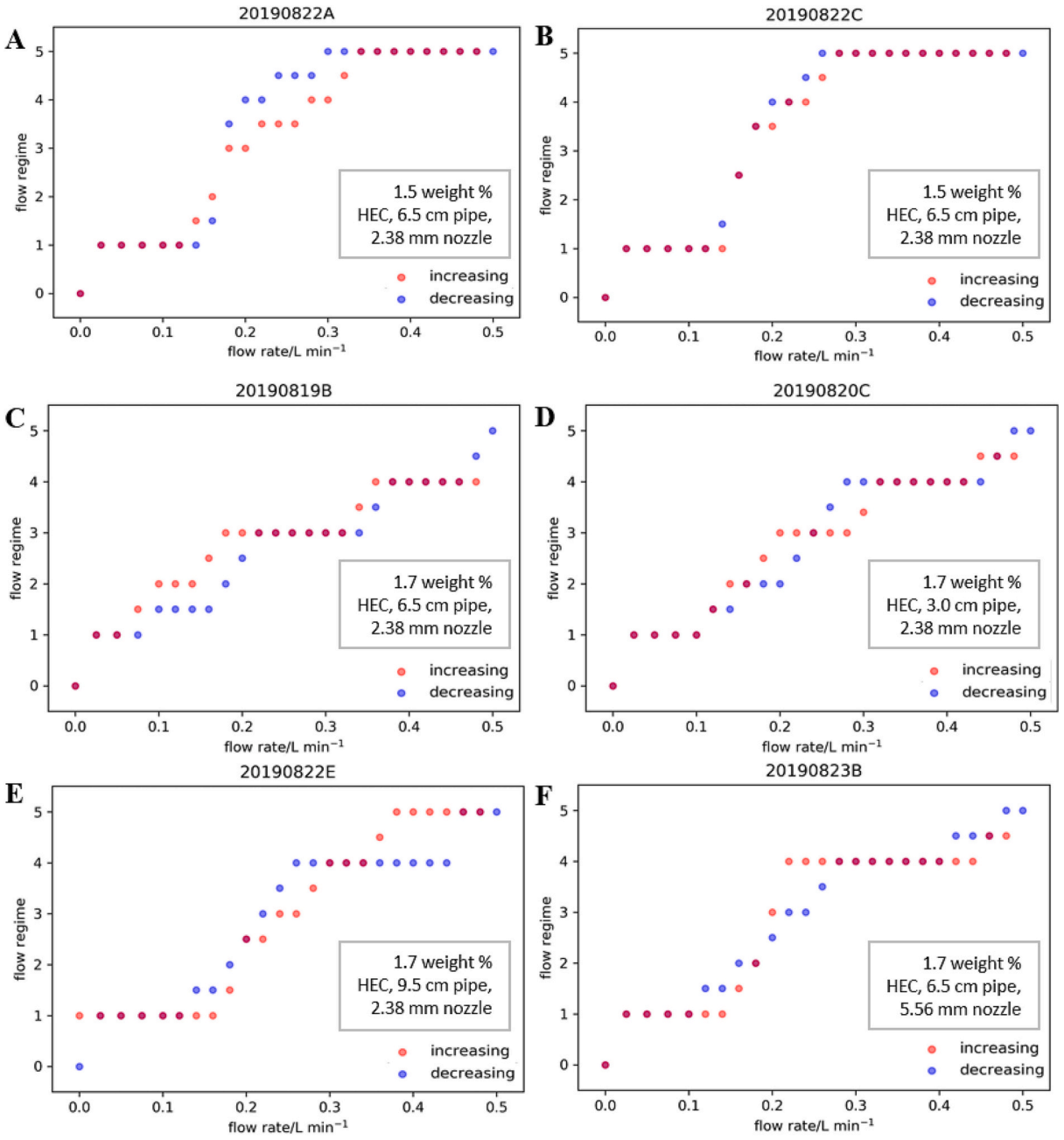

Fig. 6. Bubble flow regime against gas flow rate plots for: (A) 1.5 wt% HEC, experiment run 20190822A, (B) 1.5 wt%, experiment run 20190822C), (C) 1.7 wt% HEC, experiment run 20190819B, (D) 1.7 wt% HEC, experiment run 20190820C, (E) 1.7 wt% HEC, experiment run 20190822E, and (F) 1.7 wt% HEC, experiment run 20190823B. Red = increasing flow rate; blue = decreasing flow rate; purple = overlapping points. (For interpretation of the references to colour in this figure legend, the reader is referred to the web version of this article.)

why these different modes occurred intermittently, even when magma and gas flow rate were constant. While our study does not definitively answer this question, we have shown that gas flow rate is a key control on the way that gas travels through a non-Newtonian, shear-thinning, viscoelastic fluid. Furthermore, we find that, even under carefully controlled conditions in the laboratory, the gas transport regime is somewhat unstable, with bubble chains and flues prone to collapse, particularly if gas flow rate is perturbed sharply. When applying these studies to real volcanic systems, it would be unrealistic to assume that conditions, such as gas flow rate, are constant. This implies that gas transport regimes are more ephemeral in nature than in our experiments.

There are other differences between the laboratory and natural systems that might lead to differences in phenomenology. Firstly, we note that the gas injection nozzle used in our experiments does not have an obvious counterpart in the natural system. It is not clear, therefore, how gas would organize itself such that it could constantly feed the start of a bubble chain or flue; however, we note that nozzle diameter appears to play no role in our experiments, hence bubble chain phenomena may be relatively insensitive to the geometry of the gas feed. Secondly, a key characteristic within each of the flow regimes we observed is that the connecting neck between bubbles (flow regimes 2 and 3) are consistently narrow compared with the width of the bubble. We have found no evidence that the scale of the phenomena changes with viscosity (HEC concentration), gas flow rate, gas injection nozzle size, or pipe diameter, hence we must expect that the phenomena would have similar length

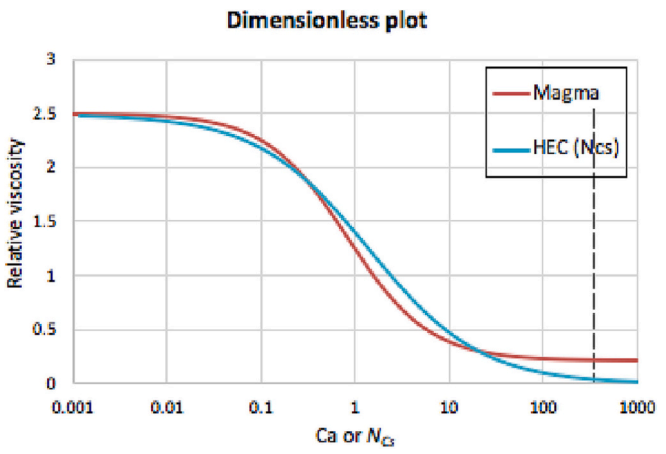

Fig. 7. Dimensionless comparison of the rheologies of a 1.7 wt% HEC solution at temperature $T = 20$ °C and a magma with a gas fraction of $\varphi = 0.6$ and a pure melt viscosity of $\mu_0 = 1000$ Pa s. The vertical black dashed line represents the maximum capillary number, Ca_{max}. The plot was created using the scaling spreadsheet provided by Jones et al., 2020.

scales in the volcanic case. Given that viscoelasticity arises at the molecular scale in polymer solutions, but at the bubble scale in bubble suspensions, it is not clear whether the viscoelastic stresses would operate at the correct scale in the natural system for the bubble chain and flue phenomena to occur. To put it another way, the local environment around a neck within a bubble chain in a bubbly magma might not exhibit the viscoelastic behaviour that is required for bubble chain phenomena to occur. Finally, we infer that wall effects may play a role in the laboratory experiments, for the smallest pipe size. In the natural system, however, these are likely to be negligible, since the size of the bubble chains would be so small compared to the size of the conduit.

Further experiments are required to establish whether bubble chain phenomena can operate in natural bubbly magmas and, if they do, how they mediate gas transport. Open questions include:

1) *Can multiple chains exist in parallel and, if so, how closely can they be spaced?* This sets a limit on the gas flux that could be transported through a body of magma. This could be investigated by employing multiple gas injection nozzles, at varying distances from each other, in future experiments. Such experiments would allow the gas flux to be compared with real measurements for degassing rates at different volcanic systems.
2) *Do the draining or whistling sounds produced by the winding flues (gas flow regime 4 in this study) relate to volcanic tremor?* A further key avenue of investigation is the relationship between gas flow through bubble chains and flues and volcanic tremor. Volcanic tremor has been observed at basaltic volcanoes, such as Etna, and is an important tool in volcanic monitoring. It has been suggested that passive degassing and volcanic tremor are coupled (Salerno et al., 2018), therefore, investigating whether gas flow via a winding flue, and associated draining or whistling sounds, is linked to volcanic tremor would be valuable.
3) *How do the complexities of natural magma – the presence of crystals, gas exsolution/dissolution, gas expansion – influence the behaviour of bubble chain phenomena?* Some of these complexities could be explored with further experiments, for example, small particles or fragments could be added to the HEC solution to represent crystals within a magma.

5. Conclusion

Overall, in this study we have (1) identified the conditions at which bubble chain phenomena occur within hydroxyethyl cellulose (HEC) solution, (2) characterised the rheology of the HEC solutions in which bubble chain phenomena successfully form, and (3) related the rheology of the HEC solutions and our experiments to basaltic magmas and volcanic systems. Our work supports the hypothesis that bubble chains could, in principle, form and produce open-system degassing in a non-Newtonian magma. However, further experiments are required to assess whether the phenomena arise and persist in bubble suspensions, for which viscoelasticity manifests only at the macroscopic scale.

Using a simple experimental set up, in which air is injected into a column of the shear-thinning fluid, HEC, we have observed and characterised five different bubble flow regimes: 1) individual bubbles with pointed tails; 2) chains of rounded bubbles connected by narrow throats (previously identified by Kliakhandler, 2002); 3) chains of elongate bubbles connected by narrow throats; 4) 'winding flues' of gas (previously identified by Divoux et al., 2009); 5) individual bubbles with pointed tails (larger than in regime 1). We varied gas flow rate, fluid viscosity/concentration, pipe size, and nozzle size and found that fluid rheology and gas flow rate were the most important factors controlling whether or not bubble chain phenomena formed, and in which regime.

Based on rheometric measurements, we conclude that the behaviour of the HEC solutions used (at 20 °C and 1.2 to 2.5 wt% concentration) are qualitatively similar to that of a magma with a relatively high gas volume fraction of $\varphi = 0.6$, with polydisperse bubble size distribution (polydisversity index = 1; Mader et al., 2013; Jones et al., 2020). Thus, the concentrations of HEC solution used in our experiments are suited for simulating shear-thinning and viscoelastic magmas. Our analysis also suggests that the shear-thinning and viscoelastic properties of HEC play a fundamental role in the observed bubble chain phenomena.

When applying this work to a real volcanic system, many questions remain open. Most importantly, our experiments show that the bubble chains are very sensitive to gas flow rate. In order to better elucidate the bubble chain mechanism, further experiments should examine the behaviour using crystal analogues, higher concentrations of HEC, as well as exploring the role of gas rate and vessel diameter.

CRediT authorship contribution statement

M. Lo: Methodology, Investigation, Writing – original draft, Visualization. **A. Loisel:** Methodology, Investigation, Writing – original draft, Visualization. **M. Burton:** Methodology, Writing – review & editing, Supervision. **E.W. Llewellin:** Methodology, Writing – review & editing, Supervision.

Declaration of Competing Interest

The authors declare no conflicts of interest relevant to this study.

Data availability

Data sets from the bubbling and rheological experiments are available here: https://figshare.com/s/4fc1c814c3d97da48f4a and https://figshare.com/s/a006d4d5283ccba5b6e1

Acknowledgements

ML thanks support from a Science and Technology Facilities Council studentship (ST/S505560/1). AL thanks support from a Durham Doctoral Studentship. EWL and MB acknowledge support from the Natural Environment Research Council via the DisEqm Large Grant (NE/N018443/1 and NE/N018575/1).

Appendix A

We can estimate the stresses exerted on the fluid by the bubbles in our experiments by considering the buoyancy force acting on them: $F_B = V\rho g$ where V is the bubble volume, ρ is the density of the liquid ($\rho \approx 1000$ kg/m^3 for all solutions), and g is gravitational acceleration. The buoyancy stress τ_B that the bubble exerts is then approximately given by the buoyancy force F_B divided by the bubble's surface area, hence

$$\tau_B = \frac{V\rho g}{4\pi R^2} = \frac{1}{3} a\rho g$$

where a is the radius of the bubble. The bubble radii in our experiments range from $1.5 \lesssim a \lesssim 12.5$ mm (see Section 3.1), hence the buoyancy stresses range from $4.9 \lesssim \tau_B \lesssim 41$ Pa. For our solutions, this stress interval falls mainly within the linear viscoelastic region, particularly for the solutions that show bubble chain phenomena (Fig. 2a). From the rotational viscometry data (Section 2.1) we can also estimate the range of strain rates that would be induced in the liquid by the buoyancy stresses. These ranges are shown in Fig. 2c and demonstrate that flow induced by bubble buoyancy falls within the region where the Cox-Merz rule holds; i.e., where there is good agreement between $\eta(\dot{\gamma})$ and $|\eta^*|(\omega)$.

Appendix B. Supplementary data

Supplementary data to this article can be found online at https://doi.org/10.1016/j.jvolgeores.2023.107874.

References

Aiuppa, A., Moretti, R., Federico, C., Giudice, G., Gurrieri, S., Liuzzo, M., Papale, P., Shinohara, H., Valenza, M., 2007. Forecasting Etna eruptions by real-time observation of volcanic gas composition. Geology 35 (12), 1115–1118. https://doi.org/10.1130/G24149A.1.

Blackburn, E.A., Wilson, L., Sparks, R.J., 1976. Mechanisms and dynamics of strombolian activity. J. Geol. Soc. 132 (4), 429–440.

Blundy, J., Cashman, K.V., Rust, A., Witham, F., 2010. A case for CO_2-rich arc magmas. Earth Planet. Sci. Lett. 290 (3–4), 289–301. https://doi.org/10.1016/j.epsl.2009.12.013.

Burgisser, A., Degruyter, W., 2015. Chapter 11 - Magma Ascent and Degassing at Shallow Levels. In: Sigurdsson, H. (Ed.), The Encyclopedia of Volcanoes, Second edition. Academic Press, Cambridge, Massachusetts, pp. 225–236. https://doi.org/10.1016/B978-0-12-385938-9.00011-0.

Burton, M., Mader, H.M., Polacci, M., 2007a. The role of gas percolation in quiescent degassing of persistently active basaltic volcanoes. Earth Planet. Sci. Lett. 264 (1–2), 46–60. https://doi.org/10.1016/j.epsl.2007.08.028.

Burton, M., Allard, P., Muré, F., La Spina, A., 2007b. Magmatic Gas Composition reveals the source Depth of Slug-Driven Strombolian Explosive activity. Science 317 (5835), 227–230. https://doi.org/10.1126/science.1141900.

Carn, S., Fioletov, V., McLinden, C., Li, C., Krotkov, N.A., 2017. A decade of global volcanic SO2 emissions measured from space. Sci. Rep. 7, 4409. https://doi.org/10.1038/srep44095.

Clift, R., Grace, J.R., Weber, M.E., 1978. Bubbles, drops, and particles. Academic, New York.

Cox, W.P., Merz, E.H., 1958. Correlation of dynamics and steady flow viscosities. J. Polym. Sci. 28, 619–622. https://doi.org/10.1002/pol.1958.1202811812.

Del Giudice, F., Tassieri, M., Oelschlaeger, C., Shen, A.Q., 2017. When Microrheology, Bulk Rheology, and Microfluidics Meet: Broadband Rheology of Hydroxyethyl Cellulose Water Solutions. Macromolecules 50, 2951. https://doi.org/10.1021/acs.macromol.6b02727.

Dinic, J., Sharma, V., 2020. Power Laws Dominate Shear and Extensional Rheology Response and Capillarity-Driven Pinching Dynamics of Entangled Hydroxyethyl Cellulose (HEC) Solutions. Macromolecules 53, 3424–3437. https://doi.org/10.1021/acs.macromol.0c00077.

Divoux, T., Bertin, E., Vidal, V., Géminard, J.-C., 2009. Intermittent outgassing through a non-Newtonian fluid. Phys. Rev. 79, 1–10. https://doi.org/10.1103/PhysRevE.79.056204.

Divoux, T., Vidal, V., Ripepe, M., Géminard, J.-C., 2011. Influence of non-Newtonian rheology on magma degassing. Geophys. Res. Lett. 38 (L12301) https://doi.org/10.1029/2011GL047789.

Francis, P.W., Burton, M.R., Oppenheimer, C., 1998. Remote sensing measurements of volcanic gas composition by solar FTIR spectroscopy. Nature 396, 567–570. https://doi.org/10.1038/25115.

Galle, B., Oppenheimer, C., Geyer, A., McGonigle, A.J.S., Edmonds, M., Horrocks, L., 2003. A miniaturised ultraviolet spectrometer for remote sensing of SO_2 fluxes: a new tool for volcano surveillance. J. Volcanol. Geotherm. Res. 119, 241–254. https://doi.org/10.1016/S0377-0273(02)00356-6.

Hansell, A., Oppenheimer, C., 2004. Health Hazards from Volcanic gases: a Systematic Literature Review. Arch. Environ. Health Int. J. 59 (12), 628–639. https://doi.org/10.1080/00039890409602947.

Houghton, B.F., Gonnermann, H.M., 2008. Basaltic explosive volcanism: Constraints from deposits and models. Geochemistry 68 (2), 117–140. https://doi.org/10.1016/j.chemer.2008.04.002.

Houghton, B.F., Wilson, C.J.N., 1989. A vesicularity index for pyroclastic deposits. Bull. Volcanol. 51, 451–462. https://doi.org/10.1007/BF01078811.

James, M.R., Llewellin, E., Lane, S., 2011. Comment on "It takes three to tango: 2. Bubble dynamics in basaltic volcanoes and ramifications for modeling normal Strombolian activity" by J. Suckale, BH Hager, LT Elkins-Tanton and J.-C. Nave. J. Geophys. Res. Solid Earth 116.

Jones, T.J., Llewellin, E.W., Mader, H.M., 2020. The use of a shear-thinning polymer as a bubbly magma analogue for scaled laboratory experiments. J. Volcanol. Geotherm. Res. 392, 1–16. https://doi.org/10.1016/j.jvolgeores.2020.106768.

Kliakhandler, I., 2002. Continuous chain of bubbles in concentrated polymeric solutions. Phys. Fluids 14 (10), 3375–3379. https://doi.org/10.1063/1.1501284.

Llewellin, E.W., Mader, H.M., Wilson, S.D.R., 2002. The constitutive equation and flow dynamics of bubbly magmas. Geophys. Res. Lett. 29 (24) https://doi.org/10.1029/2002GL015697.

Mader, H.M., Llewellin, E.W., Mueller, S.P., 2013. The rheology of two-phase magmas: a review and analysis. J. Volcanol. Geotherm. Res. 257, 135–158. https://doi.org/10.1016/j.jvolgeores.2013.02.014.

Maestro, A., González, C., Gutiérrez, J.M., 2002. Shear thinning and thixotropy of HMHEC and HEC water solutions. J. Rheol. 46, 1445. https://doi.org/10.1122/1.1516789.

Mintz, B.G., Houghton, B.F., Llewellin, E.W., Orr, T.R., Taddeucci, J., Carey, R.J., Kueppers, U., Gaudin, D., Patrick, M.R., Burton, M., Scarlato, P., 2021. Patterns of bubble bursting and weak explosive activity in an active lava lake—Halema 'uma 'u, Kīlauea, 2015 (no. 1867-E). In: US Geological Survey.

Mori, T., Burton, M., 2009. Quantification of the gas mass emitted during single explosions on Stromboli with the SO_2 imaging camera. J. Volcanol. Geotherm. Res. 188 (4), 395–400. https://doi.org/10.1016/j.jvolgeores.2009.10.005.

Naik, S.C., Pittman, J.F.T., Richardson, J.F., 1976. The Rheology of Hydroxyethyl Cellulose Solutions. Trans. Soc. Rheol. 20, 639. https://doi.org/10.1122/1.549427.

Parfitt, E.A., 2004. A discussion of the mechanisms of explosive basaltic eruptions. J. Volcanol. Geotherm. Res. 134, 77–107.

Rust, A.C., Manga, M., Cashman, K.V., 2003. Determining flow type, shear rate and shear stress in magmas from bubble shapes and orientations. J. Volcanol. Geotherm. Res. 122 (1–2), 111–132. https://doi.org/10.1016/S0377-0273(02)00487-0.

Salerno, G.G., Burton, M., Di Grazia, G., Caltabiano, T., Oppenheimer, C., 2018. Coupling between magmatic degassing and volcanic tremor in basaltic volcanism. Front. Earth Sci. 6, 157. https://doi.org/10.3389/feart.2018.00157.

Song, S.-R., Jones, K.W., Lindquist, B.W., Dowd, B.A., Sahagian, D.L., 2001. Synchrotron X-ray computed microtomography: studies on vesiculated basaltic rocks. Bull. Volcanol. 63, 252–263. https://doi.org/10.1007/s004450100141.

Van Manen, S.M., 2014. Perception of a chronic volcanic hazard: persistent degassing at Masaya volcano, Nicaragua. J. Appl. Volcanol. 3, 9. https://doi.org/10.1186/s13617-014-0009-3.

Vidal, V., Soubiran, F., Divoux, T., Géminard, J.-C., 2011. Degassing cascades in a shear-thinning viscoelastic fluid. Phys. Rev. 84, 1–9. https://doi.org/10.1103/PhysRevE.84.066302.

Wilson, L., Head, J.W., 1981. Ascent and eruption of basaltic magma on the Earth and Moon. J. Geophys. Res. 86, 2971–3001.